Electronic g Tensors in U(V) Complexes - A Computational Study

DOI:
10.1002/chem.201701058

Document Version
Accepted author manuscript

CHEMISTRY
A European Journal

A Journal of
ChemPubSoc Europe

Accepted Article

Title: Electronic g Tensors in U(V) Complexes - A Computational Study

Authors: Helen Moylan and Joseph McDouall

To be cited as: *Chem. Eur. J.* 10.1002/chem.201701058

Link to VoR: http://dx.doi.org/10.1002/chem.201701058

Supported by
ACES

WILEY-VCH

10.1002/chem.201701058

WILEY-VCH

Electronic g Tensors in U(V) Complexes - A Computational Study

Helen M. Moylan*[a] and Joseph J.W. McDouall[a]

Abstract: The theory and computation of EPR parameters from first principles has seen a great deal of development over the past two decades. In particular, various techniques for the computation of the electronic **g** tensor have been implemented in many quantum chemistry packages. These methods have been successfully applied to paramagnetic organic species and transition metal systems. The situation is less well-understood and established in the case of actinide containing molecules and there is a dearth of experimental data available for validation of computations. In this study we have used quantum chemical techniques to evaluate the **g** tensor for U(V) complexes, for which experimental data are available for comparison. The **g** tensors were calculated using, relatively simple, state averaged CASSCF calculations. We show that this approach is capable of providing useful accuracy. We discuss aspects of the computations that should be refined to provide a more quantitative approach. The key features of the underlying electronic structure that influence the computed g values are delineated, providing a simple physical picture of these subtle molecular properties.

Introduction

Computational studies of the molecular chemistry of actinide containing systems have a long history. The inherent difficulties associated with experimental work involving the actinides has recently led to an increased interest in the use of computational studies to complement and enhance our fundamental understanding of f-element chemistry.[1] The range of applications is considerable and varies: from studies of geometrically simple systems where the intention is to understand the fundamental electronic structure and bonding in actinide molecules;[2] to the use of fluorescence spectroscopy to correlate between the molecular structure (ligand species and type) with the observed spectral lineshape;[3] to studying the potential for designing actinide molecular magnets;[4] to predicting and controlling the behaviour of actinide elements in solution.[5] Understanding the origin of actinide metal to ligand selectivity is key in developing nuclear waste reprocessing techniques that separate the lanthanides from the actinides and also in facilitating the design of new extractants. These aspects of fundamental actinide chemistry are crucial to keeping the nuclear energy option open.

The theoretical description of the electronic structures of actinide molecules is intrinsically complex due to the presence of many subtle electronic effects that must be described reliably. For example, closely spaced valence orbital energy levels give rise to low-lying electronically excited states. Spin-orbit interactions are able to couple ground and excited states of different multiplicities, necessitating a multi-state approach to the electronic structure. Scalar relativistic contractions of the actinide core atomic orbitals, accompanied by the concomitant expansion of the d and f orbital manifolds, can produce profound changes in molecular properties. Additionally, many of the actinides in their most stable oxidation states have open shell electronic configurations creating paramagnetic character. These facets of the electronic structure present severe tests for current computational methods.

Experimentally, electron paramagnetic resonance (EPR) and paramagnetic nuclear magnetic resonance (PNMR) spectroscopy are used to study the physical and chemical properties of open shell species. Of particular interest is the Zeeman effect that removes the 2*S*+1 degeneracy of spin energy levels in the presence of a magnetic field, **B**. The Zeeman interaction is usually discussed using the phenomenological spin hamiltonian in which the molecular **g** 'tensor' parameterises the splitting of energy levels by the interaction between the magnetic field and the electronic spin:[6]

$$\widehat{H_{\mathrm{Z}}} = \mu_{\mathrm{B}}\mathbf{B}\cdot\mathbf{g}\cdot\mathbf{S} \qquad \textbf{(1)}$$

(The matrix **g** is not a proper rank-2 tensor, but we shall refer to it by this commonly adopted name.) Experimentally the g value measured for a magnetic field in a direction characterised by the unit vector **x** (relative to the laboratory frame) is:

$$g_{\mathbf{x}} = \pm\sqrt{\mathbf{x}\cdot\mathbf{g}\mathbf{g}^{\mathbf{T}}\cdot\mathbf{x}} \qquad (2)$$

In (2), the quantity $\mathbf{g}\mathbf{g}^{\mathbf{T}}$ is a rank-2 tensor. In molecules the shift from the free electron g value (g_{e} ≈ 2.002319) is associated with the loss or gain of orbital angular momentum and is a source of information regarding the intrinsic electronic structure of the system. Interest in **g** spans the entire range of the periodic table: from organic radicals; to transition metals; to the f-elements. In organic radicals spin-orbit coupling is often very small and covalent bonding is strong. For the f-elements spin-orbit effects are large, low lying excited states are present and covalent bonding is relatively weak. Understanding the origin of the g shifts and the factors that govern the observed spectra can lead to an improved knowledge of the fundamental chemical and electronic structure in paramagnetic systems.

Computations of g can aid the interpretation of observed EPR spectra, predict parameters that are difficult to determine experimentally and be used to explore where experiment cannot. There are a few examples of calculated g values for actinide molecules in the literature. Previous studies have largely

[a] H.M Moylan, J.J.W McDouall
School of Chemistry
University of Manchester
Oxford Road
Manchester
M13 9PL (UK)
E-mail: helen.moylan@postgrad.manchester.ac.uk
Joe.mcdouall@manchester.ac.uk

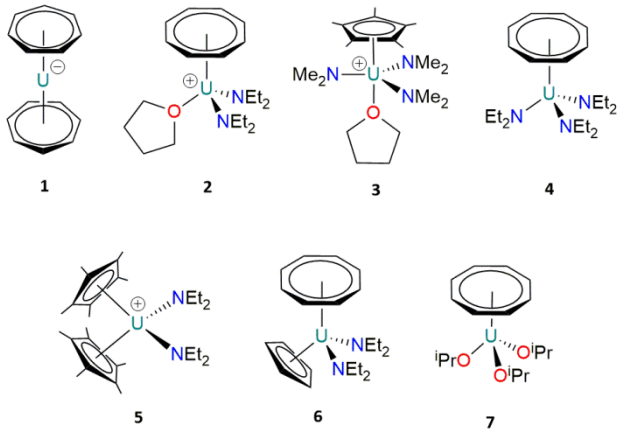

Figure 1. **1** $[U(\eta^7\text{-}C_7H_7)_2]^-$; **2** $[(\eta^8\text{-}C_8H_8)U(NEt_2)_2THF]^+$; **3** $[(\eta^5\text{-}C_5Me_5)U(NMe_2)_3THF]^+$; **4** $[(\eta^8\text{-}C_8H_8)U(NEt_2)_3]$; **5** $[(\eta^5\text{-}C_5Me_5)_2U(NEt_2)_2]^+$; **6** $[(\eta^8\text{-}C_8H_8)(\eta^5\text{-}C_5H_5)U(NEt_2)_2]^+$; **7** $[(\eta^8\text{-}C_8H_8)U(O\mathit{i}Pr)_3]$.

focused on highly symmetrical systems (AnX_6^{n-}) with isotropic g values.[7–13] Other more complex examples have been studied,[14,15] however experimental data are lacking for comparison with these calculations. Since *ab initio* calculations of g values in actinide containing compounds are relatively rare, and the computational procedure for their accurate calculation is far from routine, there is an essential need to benchmark this type of calculation against experimental data. In particular studies that focus on systems with lower symmetry (anisotropic g values) and/or multiple unpaired electrons are needed. This consideration, in part, determined the subjects of this study. Molecules **1**-**7**,[16–18] shown in figure 1, provide a set of actinide complexes that have well defined EPR spectra for the (relatively) simple $5f^1$ actinide configuration, allowing us to assess our computational protocol for the calculation of **g**. Detailed experimental analysis of the EPR spectra of **1**-**7** have been carried out by Ephritikhine *et al*.[19,20]

The computation of **g** tensors is quite well established for lighter elements, including transition metals, within the density functional theory (DFT) formalism. Linear response theory is used to include the effects of spin-orbit coupling as a first-order perturbation.[21–26] Such an approach can be successful provided the spin-orbit interaction is not too large and there are no low-lying excited states. When applicable, the linear response treatment is more efficient than including the interaction with excited states through a direct summation. We cannot expect the linear response approach to work well in cases of orbital degeneracy, or near degeneracy, nor in cases where the underlying electronic structure of the ground state is multiconfigurational (a situation that we can anticipate generally in systems with multiple metal centres, not just actinides). In actinide systems, where ligand interaction with the valence metal orbitals is weak, at least some (near) degeneracy of the 5f manifold is preserved. The magnitude of the spin-orbit coupling is also large. Hence we can anticipate difficulties for the linear response approach. Bolvin and Autschbach[27] have recently reviewed computational approaches for obtaining the **g** tensor and conclude that in the case of strong spin-orbit coupling the methods used should include spin-orbit effects to high order or, preferably, variationally.

In this study we shall concentrate on U(V) containing complexes with a $5f^1$ electronic configuration. The energy levels of odd electron systems are subject to a Kramers degeneracy and this is exploited to obtain the **g** tensor. The method used was first formulated, in an *ab initio* context, by Bolvin.[28] The spin-orbit interaction is applied first of all to obtain the wavefunctions of the degenerate Kramers pair. The energy splitting, in the presence of a magnetic field, is then obtained by diagonalising the Zeeman operator in the basis of the Kramers pair. By this process it is possible to obtain the matrix $\mathbf{g}\mathbf{g}^{\mathbf{T}}$, from which the principal values of **g** are evaluated as the positive square roots of the eigenvalues of $\mathbf{g}\mathbf{g}^{\mathbf{T}}$. The sign of the product of the resulting g values can be obtained from the electronic magnetic moments, μ_i (where *i* refers to the components of the magnetic axes of the system), evaluated in the basis of the Kramers pair. This strategy can also be used for systems in which $S \neq ½$, provided pairwise degeneracy of spin-orbit states is present. In such cases the concept of a pseudo-spin, $\tilde{S}$, is used such that $2\tilde{S} + 1 = 2$.[29] Each degenerate pair, characterised by $\tilde{S}$, may then be treated using Bolvin's scheme.

Results and Discussion

Computational Methods: Geometries

Crystal geometries are only available for some of the set of molecules, **1**-**7**.[16–18] For a consistent treatment we chose to optimise all structures studied. The presence of the U(V) ion requires that the effects of relativity are included in any computational scheme. This is often dealt with through the use of relativistic effective core potentials (RECP). We have used an all electron approach throughout this work. A particularly simple scheme for including relativistic effects involves the use of the zeroth-order regular approximation (ZORA) in Filatov's resolution of the identity formulation.[30] The necessary analytic integrals over basis functions, which are required to modify the kinetic energy in the one-electron hamiltonian, are easily obtained. To avoid issues related to gauge invariance and the evaluation of additional terms in the energy gradient and hessian the modification of the one-electron hamiltonian is applied in atomic blocks following the suggestion of van Lenthe *et al.*[31] We refer to this scheme as 'atomic' ZORA (aZORA). This allows the use of the standard apparatus, available in any quantum chemistry code, to carry out all electron relativistic geometry optimisations at negligible extra cost compared to the non-relativistic case. We have employed this aZORA scheme to obtain the optimised geometries for all molecules studied here.

For uranium we have used the segmented all electron relativistically contracted (SARC) basis set,[32] with all other atoms described by the Def2-SVP[33] basis set. The PBE0 exchange-correlation functional was used throughout. All geometry optimisations were carried out using the Gaussian suite of programs.[34] Our implementation of the aZORA scheme calls the standard integral routines within Gaussian.

In the supplementary information (SI) we have compared key geometric variables taken from the crystal structures with those obtained as described here. We find the aZORA scheme affords very reliable geometries at low computational cost. The coordinates of the optimised geometries of **1**-**7** are reported in the SI.

Computational Methods: g tensors

All **g** tensor calculations were carried out using the ORCA program[35] (version 3.0.3). (We note that the aZORA scheme described previously can also be carried out using ORCA.) Relativistic effects were included using the Douglas-Kroll-Hess transformation to second-order (DKH2).[36,37] Standard complete active space self-consistent field (CASSCF) calculations were performed with state averaging (SA-CASSCF) to yield a single set of orbitals to be used in the spin-orbit coupling treatment. It is possible to use state optimized orbitals and treat the resulting nonorthogonality problem via a transformation to biorthogonal orbitals,[38] but we have not done so in this study. The spin-orbit mean field operator, SOMF(1X) as described by Neese,[39] was used to include spin-orbit coupling via quasi-degenerate perturbation theory (QDPT) applied to the CASSCF states. Picture change transformation of the spin-orbit operator was included to second-order in the DKH scheme, and to first-order for the Zeeman operator.[40] Again the SARC basis set was used for uranium (contracted for the DKH method). All other atoms used the Def2-TZVP[33] basis set. Density fitting approximations were used to reduce the computational burden in calculating the spin-orbit integrals and also the integral transformation used in the CASSCF calculation.

It should be noted that the **g** tensors have been calculated in the gas phase. The optimised geometries have also been obtained in the gas phase. In contrast the EPR experiments were conducted on frozen solutions. We have made no attempt to model the influences of the environment on the computed **g** tensors.

Detailed Case Studies: $[U(\eta^7\text{-}C_7H_7)_2]^-$, 1

The bis(cycloheptatrienyl)uranium anion, **1**, has been studied experimentally by Ephritikhine and coworkers.[18] EPR measurements, in frozen solution, of the g values and hyperfine coupling constants have been performed.[20] Our geometry optimisations were performed without any symmetry constraints. We obtained a structure in which the two cycloheptatrienyl rings are staggered with respect to each other and the molecule has axial symmetry (numerically). We note that the crystallographic geometry possesses C_{2h} symmetry but consideration of the states of this molecule are better described in D_{7d}, D_{7h} or D_7 symmetry, as discussed by Li and Bursten.[41] The staggered conformation of the rings (D_{7d}) with the single f electron occupying the uranium $5f_{z^3}$ orbital gives the ground electronic state as A_{2u}.The experimentally measured g values show substantial shifts from g_e, being $g_\perp$ = 2.365 and $g_\parallel$ = 1.244.

Table 1. g values obtained for **1** using various exchange-correlation functionals. Basis sets: U (SARC), all other atoms (Def2-TZVP). DKH2 relativistic treatment with picture change transformations included.

	% Exact Exchange	$g_\perp$	$g_\parallel$
Experiment[20]	–	2.365	1.244
VWN[42]	0	1.84	2.00
BP86[43,44]	0	0.071	0.23
PBE[45,46]	0	0.067	0.19
TPSSh[47]	10	0.059	1.99
B3LYP[42,48–50]	20	1.12	1.98
PBE0[51]	25	1.46	1.98
BHHLYP[48]	50	2.71	1.92

To begin we investigated the performance of DFT with a range of exchange-correlation functionals. The **g** tensor was obtained with the linear response formalism,[26] as implemented within the ORCA program, using large quadrature grids and tight convergence criteria. Table 1 lists the g values obtained. We found that DFT calculations on **1** often converged to a solution that did not correspond to the global energy minimum. This was checked for each functional, by swapping the singly-occupied f orbital, to ensure that the global minimum was obtained. The range of g values obtained varies unpredictably with the nature of the exchange-correlation functional used. All functionals studied here, with the exception of BHHLYP, predict the magnitudes of $g_\perp$ and $g_\parallel$ in the opposite order to experiment, with $g_\parallel > g_\perp$. There appears to be a direct correlation between the quantity of exact exchange included in the hybrid functionals and the magnitude of $g_\perp$. However, the generalised-gradient functionals, with no exact exchange, appear to contradict this trend with $g_\perp$ being predicted to be 0.071 (BP86) and 0.067 (PBE). The computed values of $g_\parallel$ are much less sensitive to the nature of the exchange-correlation functional, but mostly $g_\parallel$ is predicted to be too large in magnitude. This poor description of the **g** tensor may be due to the linear response treatment of the spin-orbit coupling, rather than a specific failing of the DFT approach. A recent review of the computation of EPR parameters[27] concludes that higher-order treatment of spin-orbit coupling (beyond linear response) is essential for heavy elements.

In actinide systems, the 5f orbitals are not significantly perturbed by the surrounding ligands, preserving the degeneracy of these orbitals to some extent and potentially leading to multiconfigurational character of the electronic structure. Since **g** is a property of the valence electrons, the poor treatment of non-dynamic electron correlation in single reference DFT could explain the inadequacy of this approach for accurately describing **g** in these systems. Another consideration here is that, as will be seen, there exist several low lying excited states which are key to a proper description of **g** in these systems. The DFT formalism optimises the description of the ground state. Accordingly, we have employed the state averaged CASSCF approach in our studies so that we may better describe both ground and excited states on a more equal footing.

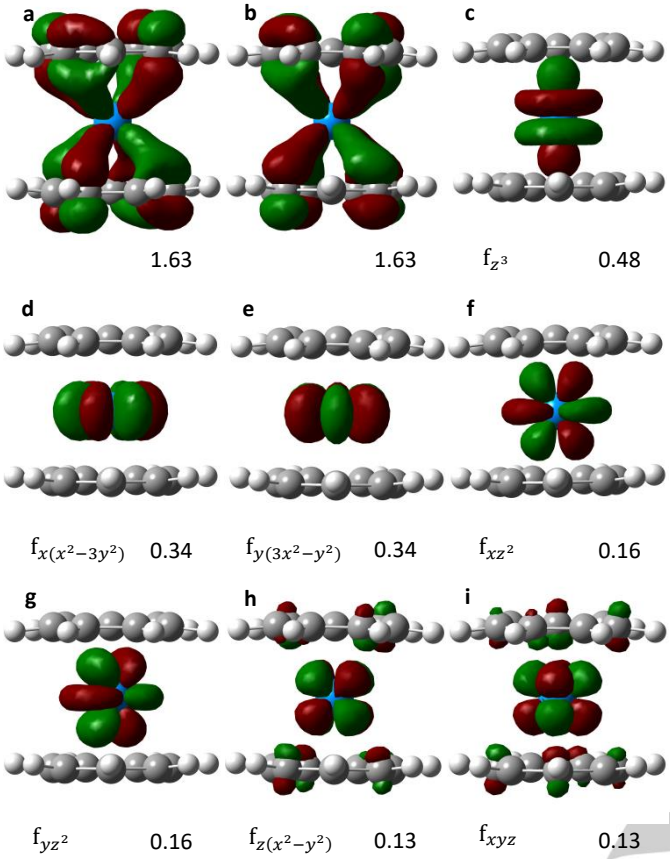

Figure 2. SA-CASSCF(5,9) active space orbitals of **1** obtained with 15 states averaged. The natural orbital occupation numbers and orbital labels are shown below each orbital.

The choice of active space must include, as a minimum, the full f orbital manifold of the U atom. There is no simple and reliable procedure for assessing which, if any, additional orbitals should be included in the active space. The technique we have used to assess the potential participation of orbitals in the active space is based on the spin-unrestricted natural orbitals (UNO)[52] obtained from the Kohn-Sham density computed with the PBE0[51] exchange-correlation functional. For each system studied the active space was chosen after analysis of the natural orbitals and their occupation numbers. In particular we looked for orbitals where significant interaction between the ligands and the uranium f orbitals occurs. In the case of **1** the natural orbitals showed depopulation of two bonding orbitals, centred mainly on the ligands, into two antibonding orbitals that contained large components of uranium f orbital character. Including these two orbitals and their electrons in addition to the f orbitals on uranium leads to a five-electron, nine-orbital (5,9) active space. Since we must consider the role of excited states SA-CASSCF(5,9) calculations were then performed, varying the number of states included in the state averaging process. The number of states included was explored empirically, by increasing the number of states until some convergence in the results was seen. The ground state is singly degenerate with the lowest excited states appearing as degenerate pairs. The number of roots included in the state averaged calculation therefore reflects this, to avoid separating any degenerate states. Figure 2 shows the SA-CASSCF(5,9) orbitals obtained when 15 states are state averaged.

The ground state wavefunction is dominated (75%) by a configuration in which the ring bond orbitals ((a) and (b) in figure 2) are doubly occupied with one electron in the uranium f_{z^3} orbital ((c) in figure 2). The only other significant configurations correspond to two excitations from the ring bond orbitals to the uranium $f_{z(x^2-y^2)}$ and f_{xyz} orbitals ((h) and (i) in figure 2), each contributing 9%. These latter configurations persist in the wavefunctions of the lowest few excited states contributing between 7%-9% each. The leading contribution in each of these excited states corresponds to the single electron occupying different components of the f orbital manifold, namely the ligand field states of the metal ion. The eighth and ninth states are dominated (91%) by excitations from the ring bond orbitals to the uranium $f_{x(x^2-3y^2)}$ and $f_{y(3x^2-y^2)}$ orbitals ((d) and (e) in figure 2).

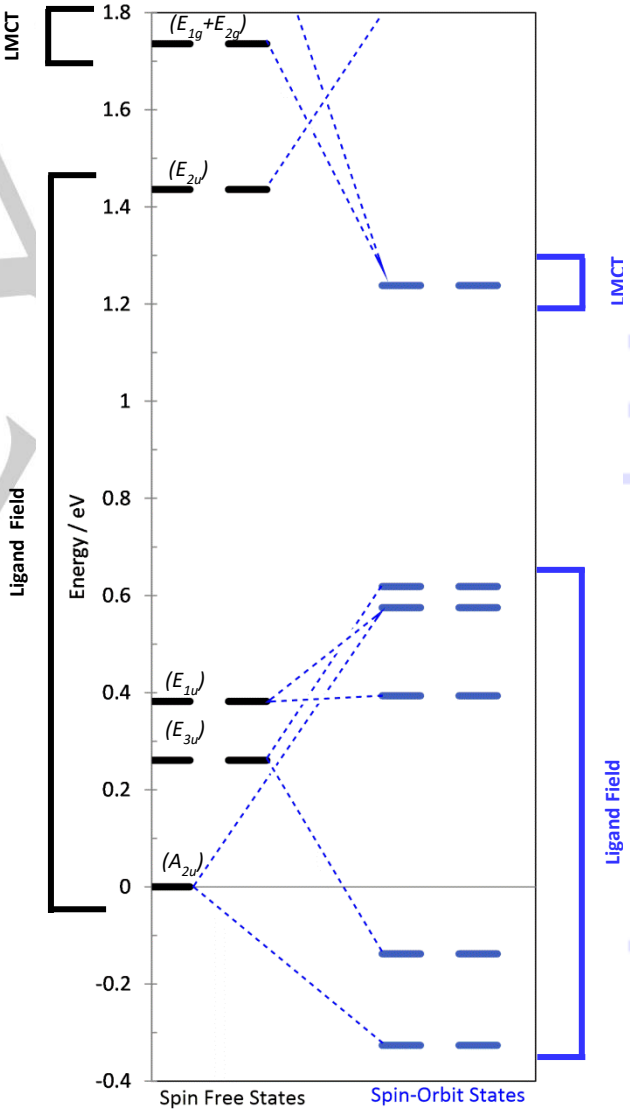

Figure 3. SA-CASSCF(5,9) electronic states of **1** and the corresponding (QDPT) spin-orbit states. Spin free states are labelled according to a simple group description in D_{7d} symmetry.

These states can be thought of as ligand to metal charge transfer states (LMCT).

Considering now the **g** tensor, shifts from the free electron g value are caused by mixing of the molecular ground state with electronically excited states through spin-orbit coupling. The distribution of the lowest few spin free and spin-orbit states are shown in figure 3. The genealogy of the spin-orbit states is indicated and may be extracted from the eigenvectors of the QDPT spin-orbit hamiltonian. In figure 3, for both the spin free and the spin-orbit states, the highest energy degenerate pair of states shown correspond to LMCT states. All lower energy states shown are local ligand field states. The spin-orbit coupling operator will, in principle, couple states with $\Delta S = 0, \pm 1$. The molecules **1**-**7** contain the U(V) ion $(S = 1/2)$, implying that doublet and quartet states will all interact. However a perturbation analysis of the **g** tensor shows that states with spin different to that of the ground state do not contribute to the **g** tensor to second-order in perturbation theory.[53] In the technique used in the present study, the **g** tensor elements are obtained from expressing the Zeeman operator in the basis of the Kramers pair. Thus the inclusion of quartet states can influence the outcome through the state averaging process, as this will affect the spectrum of electronic levels and the orbitals from which the states are built. However *a priori* we do not expect this effect to be large. Table 2 shows the dependence of the computed g values on the number of states included in the state averaging process. **1** exhibits an axial **g** tensor giving experimental values of $g_\perp = 2.37$ and $g_\parallel = 1.24$.[20] We find that $g_\parallel$ is quite insensitive to the level of state averaging and gives a very small spread of values, $g_\parallel = 1.22 - 1.27$. For $g_\perp$ the range of values, $g_\perp = 2.35 - 2.65$, is more dependent on the state averaging. Two local regions of convergence are seen; when 15 or lower states are included $g_\perp = 2.3 - 2.4$ and when more than 15 states are included, $g_\perp = 2.5 - 2.6$. In comparison with the experimental numbers the best agreement is obtained when 15 states are averaged. The effect of including quartet states in the spin-orbit interaction step of the calculation was also assessed and it can be seen (table 2) that the consequences are numerically very small for the g values, as anticipated in the discussion above.

Table 2. g values of **1** as a function of the number of states included in the state averaging process. Experimental values[20] are shown in parentheses.

No. States Averaged		$g_\perp$	$g_\parallel$	g_{av}
S = 1/2	*S* = 3/2	(2.37)	(1.24)	(1.99)
5		2.38	1.26	2.01
7		2.37	1.26	2.00
9		2.39	1.26	2.01
11		2.35	1.27	1.99
11	11	2.35	1.24	1.98
13		2.35	1.27	1.99
15		2.36	1.26	1.99
17		2.51	1.25	2.09
19		2.53	1.24	2.10
21		2.62	1.25	2.16
31		2.64	1.23	2.17
31	31	2.65	1.22	2.17
41		2.58	1.24	2.13
51		2.57	1.23	2.12
51	51	2.59	1.23	2.14
61		2.58	1.23	2.13
71		2.57	1.23	2.12
71	71	2.60	1.22	2.14
81		2.55	1.24	2.11
91		2.55	1.24	2.11
101		2.54	1.25	2.11
111		2.59	1.23	2.14
121		2.59	1.24	2.14
131		2.62	1.23	2.16
141		2.63	1.23	2.16
151		2.64	1.23	2.17

The choice of active space is crucial to the accuracy of the **g** tensor calculation. Interactions between ligand and actinide orbitals are generally weak. Hence an active space solely containing the 5f manifold might be thought to be a sufficiently accurate approximation of the valence electronic structure. However, in the case of **1**, carrying out such a SA-CASSCF(1,7) calculation including all seven doublet states yields the values $g_\perp = 1.69$ and $g_\parallel = 1.36$. The shifts from the free electron value are both predicted to be negative, in contrast to the experimental evidence. The inclusion of the ring δ-bonding interaction between the rings and the metal (figure 2) appears essential for an accurate description of the electronic structure, and consequently the accurate prediction of **g**. As we have mentioned previously there is no panacea for the selection of active spaces but, in this case at least, the UNO approach appears to have been successful.

To understand the dependence of the g values on the underlying electronic structure we performed small geometrical displacements of the molecular geometry and looked to see how the changes affected the computed g values and the underlying orbitals and electronic states. Denoting the centroids of the heptatrienyl rings as ⊙, we varied both U–⊙ distances simultaneously. Figure 4 shows how the g values vary as a function of the displacement of the U–⊙ distances from

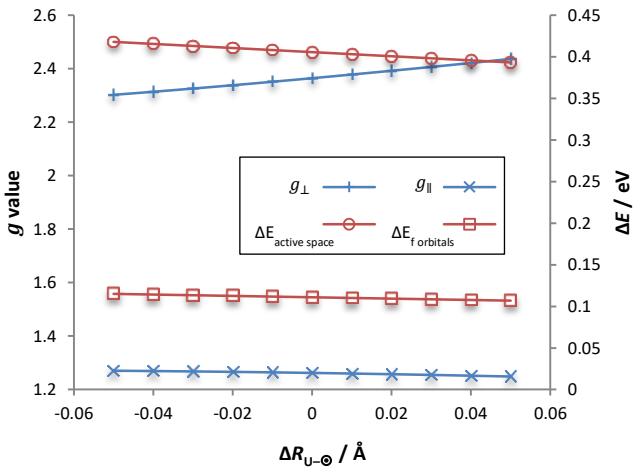

Figure 4. Changes in g values and separation in energies of orbitals shown in figure 2(a) and 2(i) of **1** at the SA-CASSCF(5,9) level with respect to displacement of the U–⊙ distances from equilibrium (see text).

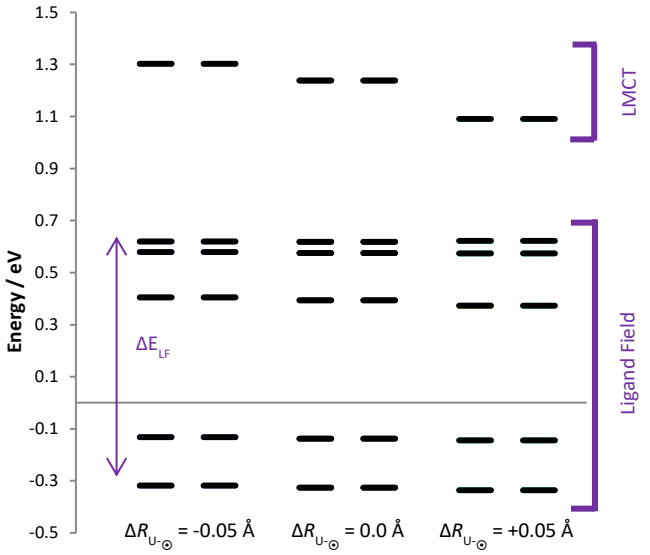

Figure 5. Changes in the spectrum of spin-orbit states of **1** at the SA-CASSCF(5,9) level with respect to displacement of the U–⊙ distances from equilibrium (see figure 3 and text).

equilibrium. $g_{\parallel}$ shows very little dependence on the U–⊙ distance but $g_{\perp}$ changes significantly, increasing in value with a positive displacement of the rings. There is a strong correlation between the behaviour of the g values and the spread of orbital energies in the active space. Also plotted in figure 4 is the difference in energy between the highest and lowest orbital in the active space (red circles in figure 4). The lowest energy orbitals correspond to the ring bonding orbitals and the highest orbitals to their antibonding counterparts (mostly centred on U, as discussed above). As these orbitals move closer together in energy their interaction increases and so does the value of $g_{\perp}$. The remaining uranium f orbitals do not show any significant change in their relative energies (red squares in figure 4) and echo the behaviour of $g_{\parallel}$ with respect to changes in the U–⊙ distance. The strong dependence of $g_{\perp}$ on the ring bond orbitals again argues for the importance of including them in the active space. This bonding/antibonding (covalent) interaction appears to be key in determining the value of $g_{\perp}$. We can also analyse this effect at the level of the spectrum of state energies. A second-order perturbation analysis of the **g** tensor elements shows that the magnitude of the shifts depends inversely on the energy separation between spin-orbit coupled states. Figure 5 shows the behaviour of the spin-orbit states as the U–⊙ distance is displaced by ± 0.05 Å. Broadly speaking we see a very gentle spread in the energies of the ligand field states, as the U–⊙ distance is increased, (ΔE_{LF} = 0.938 eV when $\Delta R_{U\text{-}\odot}$ = -0.05 Å and ΔE_{LF}= 0.958 eV when $\Delta R_{U\text{-}\odot}$ = +0.05 Å) in correspondence with the small decrease observed in the $g_{\parallel}$ values. These changes appear to be determined by the energy of the ligand field state at approximately 0.40 eV. We see a much stronger decrease in the energy of the LMCT states, as the U–⊙ distance is increased, and this parallels the more marked increase in the magnitude of $g_{\perp}$.

$[U(\eta^5\text{-}C_5Me_5)_2(NEt_2)_2]^+$, 5

The next example for detailed analysis is $[U(\eta^5\text{-}C_5Me_5)_2(NEt_2)_2]^+$, **5**. It was chosen to contrast with the previous example. The experimentally measured g values for this rhombic system are $g_1 = 0.99$, $g_2 = 1.95$, $g_3 = 2.46$.[19] Analysis of the UNO computed with the PBE0 functional showed no obvious orbitals for inclusion in the active space. The occupation numbers implied essentially doubly-occupied orbitals, followed by one singly-occupied f orbital and then the unoccupied space. Two weak bonding interactions between the uranium f orbitals and nitrogen atoms can be seen in the doubly-occupied space. We attempted to include these two interactions in the active space alongside the seven f orbitals on uranium to create a (5,9) active space. However these two doubly-occupied orbitals do not exhibit partial occupancy unless large levels of state averaging are included to cause artificial depopulation from the doubly-occupied to the f orbital space. We also attempted to include the C_5Me_5 ring—U bond orbitals in the active space, but again found the CASSCF calculation showed no depopulation away from double occupancy. This leads to the well-known redundant coordinate problem that can plague CASSCF calculations. Hence we decided on a (1,7) active space and carried out the SA-CASSCF calculations state averaging over all seven ligand field states. Figure 6 shows the SA-CASSCF(1,7) orbitals obtained.

The ground state wavefunction is dominated (57%) by an electronic configuration where the unpaired electron is in orbital (e) from figure 6. There are also significant contributions from configurations with the electron in orbital (d) (23%) and orbital

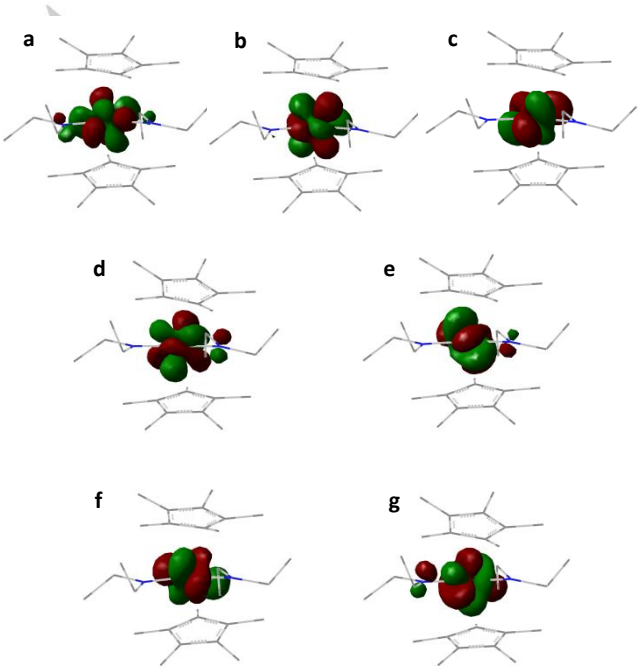

Figure 6. SA-CASSCF(1,7) active space orbitals of **5**, obtained with 7 states averaged (all orbitals have occupancy of 0.14). For clarity H atoms have been omitted and the structure drawn in wireframe. The orbital lobes that resides away from the central atom in (a), (d), (e) and (g) are all located on the N atoms.

(b) (14%). A similar pattern is seen in the other SA-CASSCF states, each having one dominant electron configuration and two other configurations contributing significantly.

The calculated g values for this system are g_1 = 1.08, g_2 = 1.33 and g_3 = 2.25 which can be compared with the experimentally determined values noted above. We found that g_1 and g_3 exhibit good agreement with the experiment, but g_2 is underestimated. In all three cases, the computed values predict the correct positive or negative shift from g_e. Figure 7 shows the SA-CASSCF(1,7) electronic states of **5** along with the resulting spin-orbit states. Comparing with the situation in **1**, (figure 3) it can be seen that the ligand field states in this case are much more closely spaced (an energy span of 0.73 eV in **5** versus 1.45 eV in **1**).

As with **1**, we conducted an analysis of the g values with respect to geometric perturbations. **5** is structurally more

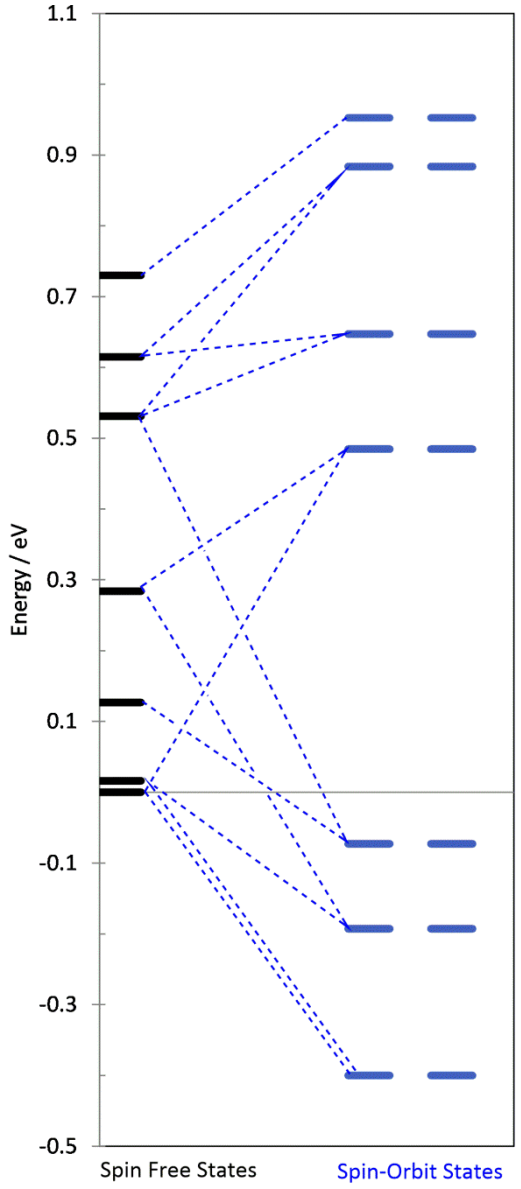

Figure 7. SA-CASSCF(1,7) electronic states of **5** and the corresponding (QDPT) spin-orbit states.

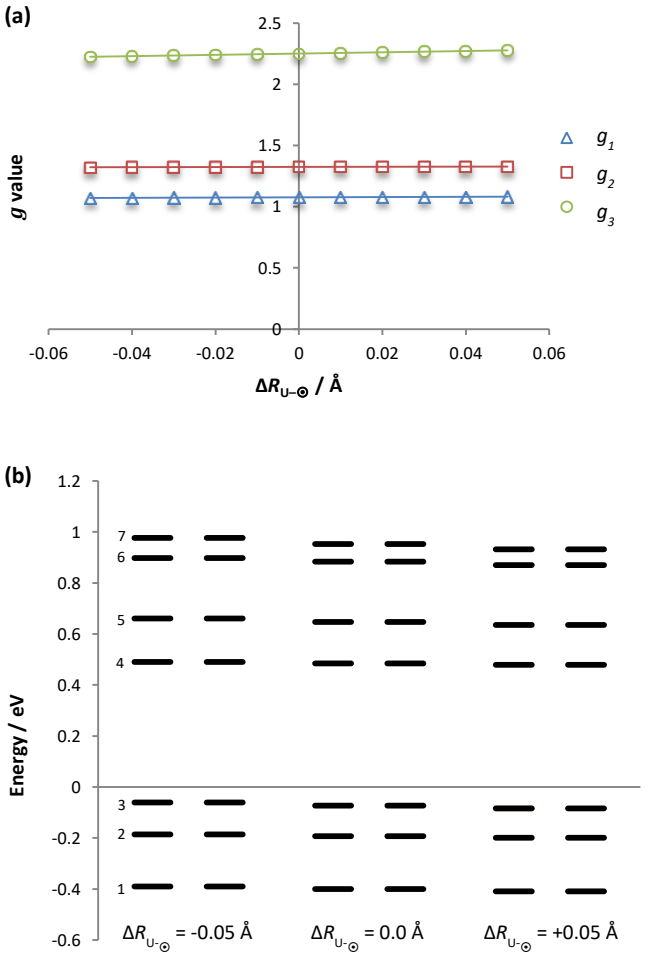

Figure 8. Changes of (a) g values and (b) energies of the spin orbit states, of **5** with respect to displacement of the U–⊙ distances from equilibrium. ⊙ represents the centroid of the C_5Me_5 rings.

complex than **1**, as the molecule contains two amide and two C_5Me_5 ligands. To perform the analysis the pair of C_5Me_5 ring centroids or the pair of amide ligands were translated in steps of ±0.01 Å from uranium. The g values were re-evaluated at the displacements and figures 8(a) and 9(a) show the results.

We then looked for correlations between the geometric perturbations and the spin-orbit states. Figures 8(b) and 9(b) show the spin-orbit states at the equilibrium geometry and ±0.05 Å for translation of the C_5Me_5 rings and the amide ligands respectively. Inspection of figure 8(a), shows that translation of the C_5Me_5 ligands has a very small effect on the calculated g values along all three principal axes. In each, the gradient is small and positive, specifically $dg_1/d\Delta R = 0.11$, $dg_2/d\Delta R = 0.06$ and $dg_3/d\Delta R = 0.52$. Figure 8(b) shows that the energies of all the spin orbit states decrease in energy as the C_5Me_5 rings are translated away from uranium. The most notable change is for the highest spin orbit states; states 6 and 7. By focusing on the difference in energy of the spin orbit states, we note that $\Delta E_{7\text{-}6}$ decreases with positive displacement of the rings ($\Delta E_{7\text{-}6}$ = 0.079 eV when $\Delta R_{U\text{-}\odot}$ = -0.05 Å and $\Delta E_{7\text{-}6}$ = 0.062 eV when $\Delta R_{U\text{-}\odot}$ = +0.05 Å). The change in $\Delta E_{5\text{-}4}$ is less pronounced ($\Delta E_{5\text{-}4}$ = 0.164 eV when $\Delta R_{U\text{-}\odot}$ = -0.05 Å and $\Delta E_{5\text{-}4}$ = 0.156 eV when $\Delta R_{U\text{-}}$

$_{\odot}$ = +0.05 Å) and $\Delta E_{3\text{-}2}$ even less so ($\Delta E_{5\text{-}4}$ = 0.125 eV when $\Delta R_{U\text{-}\odot}$ = -0.05 Å and $\Delta E_{5\text{-}4}$ = 0.115 eV when $\Delta R_{U\text{-}\odot}$ = +0.05 Å). Bearing in mind the different gradients of g value axes in figure 8(a), it seems appropriate to associate the change in g_3 with the changes in spin-orbit states 6 and 7, g_2 with states 4 and 5 and g_3 with states 2 and 3.

A similar analysis can be done with the amide ligands. In figure 9(a), g_1 and g_2 exhibit an increase in magnitude as the amide ligands move away from the uranium centre and g_3 decreases. The change in g_3 is in direct contrast to the effect caused by the C_5Me_5 ligands. When looking at the spin-orbit states in figure 9(b), we can see that similar to figure 8(b), the energies of all the spin-orbit states decrease as the ligands are displaced. However this time, there is an increase in $\Delta E_{7\text{-}6}$ with positive displacement from uranium ($\Delta E_{7\text{-}6}$ = 0.063 eV when $\Delta R_{U\text{-}\odot}$ = -0.05 Å and $\Delta E_{7\text{-}6}$ = 0.081 eV when $\Delta R_{U\text{-}\odot}$ = +0.05 Å). This interaction can once again be associated with g_3. Lower in the manifold, $\Delta E_{5\text{-}4}$ decreases as the ligands are displaced ($\Delta E_{5\text{-}4}$ = 0.19 eV when $\Delta R_{U\text{-}\odot}$ = -0.05 Å to $\Delta E_{5\text{-}4}$ = 0.14 eV when $\Delta R_{U\text{-}\odot}$ = +0.05 Å) and can again be associated with g_2 and the positive gradient of 2.5 shown in figure 2(a). $\Delta E_{3\text{-}2}$ again exhibits an increase in value as the amide ligands are displaced but is less pronounced than the effects on $\Delta E_{5\text{-}4}$, mirroring the effects seen in g_1.

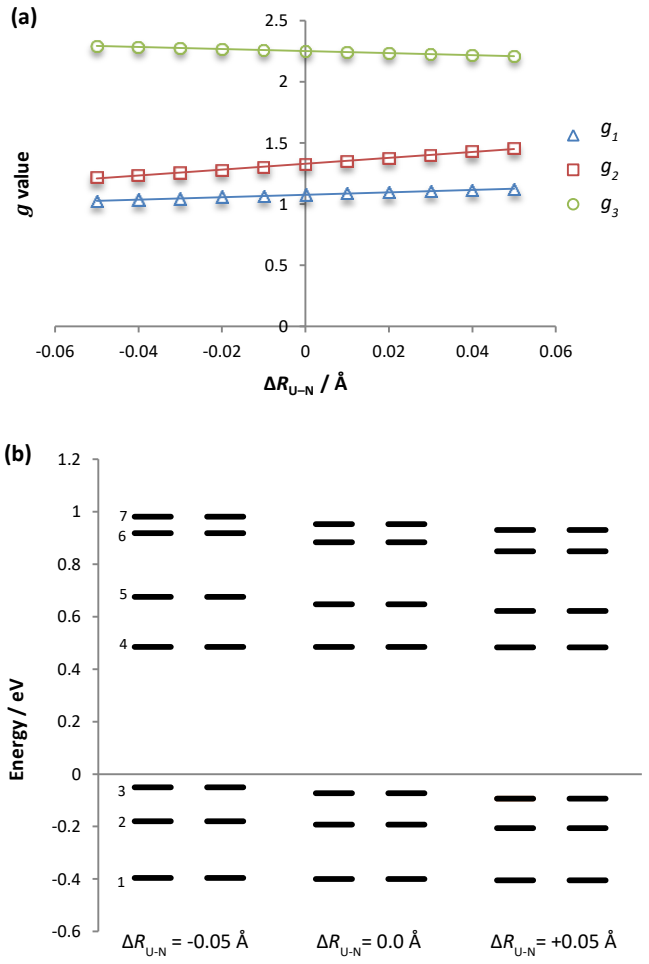

Figure 9. Changes of (a) g values and (b) energies of the spin orbit states, of **5** with respect to displacement of the U–N distances from equilibrium.

Table 3. Best estimates of computed g values for **1**-**7**, experimental values are shown in parentheses.

Molecule	Active Space / No. States	g_1	g_2	g_3
1	(5,9) / 15 states	1.26	2.36	2.36
		(1.24)	(2.37)	(2.37)
2	(5,9) / 50 states	0.10	1.02	3.18
		(0.96)	(1.64)	(3.17)
3	(1,7) / 7 states	0.16	0.91	3.14
		(<0.8)	(1.26)	(3.27)
4	(5,9) / 50 states	0.94	1.24	1.62
		(1.36)	(1.82)	(2.31)
5	(1,7) / 7 states	1.08	1.33	2.25
		(0.99)	(1.95)	(2.46)
6	(5,9) / 50 states	0.14	1.63	2.66
		(0.90)	(1.46)	(2.16)
7	(5,9) / 10 states	0.07	1.16	1.27
		(0.74)	(0.91)	(0.91)

These perturbations show the effects of different ligand groups on the electronic structure and in determining the g values. The contrasting behaviour of g_3 and the sixth and seventh pairs of spin-orbit states is indicative of this. These spin-orbit states originate from a mixing of spin free states that are dominated by electron configurations where the unpaired electron is in orbital (a), (d) and (g) from figure 6. By visualising these orbitals we can see the appearance of a small, albeit important, nitrogen component.

Summary of results for molecules 1-7

Following the general approach outlined in the previous section for the cases of **1** and **5** we collate here the results obtained for all molecules, **1**-**7**. The details for each molecule are provided in the SI.

Table 3 summarises our best estimate of all the g values. Figure 10 shows the level of agreement we obtained with

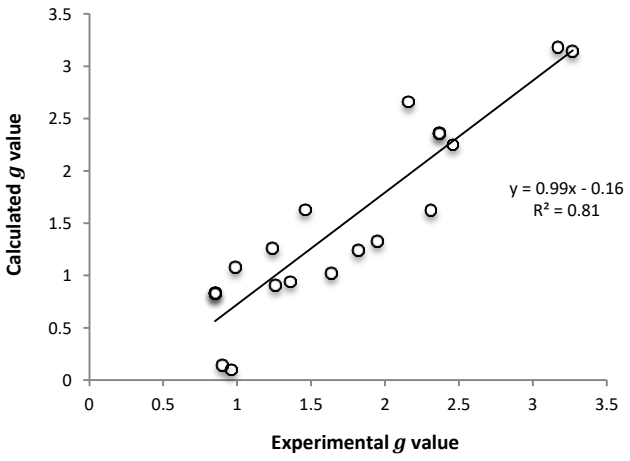

Figure 10. Correlation between the experimentally determined g values and the calculated g values for **1**-**7**.

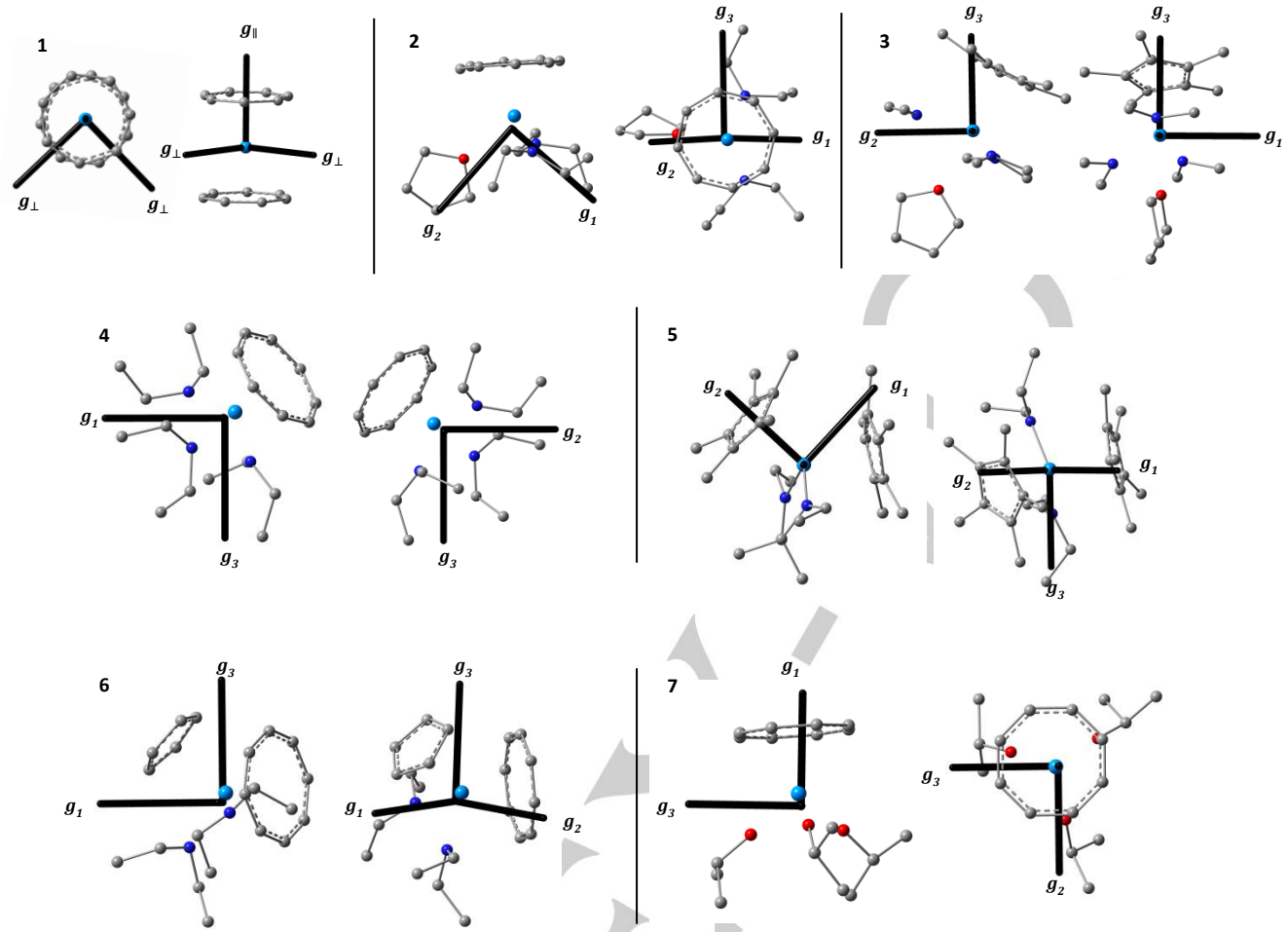

Figure 11: Axes of the **g** tensor for molecules **1**-**7**. The level of the calculation corresponds to that shown in table 3.

respect to experiment and figure 11 shows the axes of the **g** tensors for **1**-**7** superimposed on their molecular structure.

Overall a good agreement is found. It should be borne in mind when inspecting figure 10 that there are obvious limitations associated with the computed g values related to the omission of environmental factors inherent in the experiments. For example, the geometry of the molecules in a frozen solution used in the experiments versus the gas phase optimised structures used in the calculations. Additionally, the calculations have not included any treatment of the solvent environment, nor any effects of vibrational motion or temperature and the CASSCF calculations used here do not treat the dynamic electron correlation problem. The computational cost of a more extended treatment of electron correlation was deemed to be excessive in the context of this study. That said, we find a regression coefficient of R^2 = 0.81 and the line of best fit shows a gradient of 0.99.

There are two main outliers evident in the results, g_1 for molecules **2** and **6**, both of which are significantly underestimated, implying an excessive computed g shift from the free electron value. Including a very large number of states in the in the state averaging process for **2** can improve the agreement of the g_1 and g_2 values, but this has a detrimental effect on the g_3 value (see SI table S10). For **6**, all g values are improved by including large numbers of states. We can only conclude that the subtleties of the electronic structure for these molecules are not sufficiently well described at the SA-CASSCF(5,9) level of theory we have used here. Possibly a more extended treatment of the correlation problem, for example through the use of restricted active space (RAS) type methods, might remedy this. We note that if these outliers are removed from the dataset, the regression coefficient is only slightly improved to R^2 = 0.84 (gradient = 0.98).

Some care should be exercised in comparing with the available experimental data. We note that the experimental spectrum of **3** exhibits only two turning points.[19] The third is believed to appear at a field greater than 810 mT giving an upper limit for this g value of 0.8. Our calculated value is 0.16, which agrees with the implied limit, but it is difficult to say anything more precise about this value. The experimental spectrum of **7** shows one extremely broad peak at high field with the g values determined as g_1 = 0.74, g_2 = 0.91 and g_3 = 0.91.[19] The average g value is 0.85. The calculations also predict a **g** tensor at high field with the individual g values all shifting to

lower than g_e. Our calculated values are g_1 = 0.07, g_2 =1.16, g_3 = 1.27 and g_{av} = 0.83. As the experimental spectrum of **7** is unresolved, it appears better to compare g_{av} values in this case.

Conclusions

Geometries of **1**-**7** were optimised at the DFT level (PBE0 functional) using all electron basis sets and one-centre approximations to the ZORA one-electron hamiltonian ("aZORA"). The experimental crystal geometries are well reproduced by this ground state DFT method. The spin dependent **g** tensor is poorly reproduced within the linear response DFT formalism and hence we have studied the **g** tensors using simple CASSCF methods. State averaging was used to yield a single set of orbitals to describe all electronic states. Spin-orbit coupling was included at the QDPT level, employing the SOMF(1X) operator. The electronic **g** tensors were calculated using the method of Bolvin.[28]

Application of these techniques has shown generally good agreement with the available experimental g values. We have analysed the key features of the electronic structure upon which the g values depend by carrying out small geometric perturbations of the molecular structures. This allows us to relate the changes in electronic structure with the changes in the g values giving a simple intuitive interpretation of the effects.

The molecules, **1**-**7**, are all S = ½ systems and as such are amenable to study of the **g** tensor using Bolvin's method, which depends on the presence of a Kramers degeneracy. Extension of this type of study to systems with integer spin values will require an alternative approach,[e.g.][54] unless accidental pair degenerate states appear in the spectrum of electronic states which allow the use of the current methodology (on pseudospin-½ pairs of states). We are currently investigating some U(IV) systems and looking at available strategies for their treatment which we shall report in a subsequent study.

Recent reviews[27] have highlighted the need for higher-order treatment of spin-orbit effects in the computations of EPR parameters for actinide systems. As such methods become more readily available, the study of molecules containing heavy elements will become more reliable and quantitative. That said, we have shown in this work that useful accuracy can be obtained for the **g** tensors of U(V) complexes using relatively simple and well-established computational methods. Equally importantly we can delineate the key features of the underlying structure that influence the computed values, providing a simple physical picture of these subtle molecular properties. However for further validation of computational techniques a more extended set of reliable experimental data is needed for comparison.

Acknowledgements

HMM thanks the Nuclear FiRST Doctoral Training Centre and the EPRSC for the award of a studentship during which this work was carried out. The authors also thank IT services (University of Manchester) for the provision of time on the RedQueen and Computational Shared Facilities. The authors thank Prof. David Collison (University of Manchester) for useful discussions on the details of EPR experiments.

Keywords: uranium complexes • electronic g tensor • Electronic structure • quantum chemistry • molecular structure and bonding

[1] M. Dolg, Ed. , *Computational Methods in Lanthanide and Actinide Chemistry*, Wiley, Chichester, **2015**.

[2] B. Vlaisavljevich, L. Andrews, X. Wang, Y. Gong, G. P. Kushto, B. E. Bursten, *J. Am. Chem. Soc.* **2016**, *138*, 893–905.

[3] B. Drobot, R. Steudtner, J. Raff, G. Geipel, V. Brendler, S. Tsushima, *Chem. Sci.* **2015**, *6*, 964–972.

[4] S. T. Liddle, J. Van Slageren, in *Lanthanides Actinides Mol. Magn.* (Eds.: R.A. Layfield, M. Murugesu), Wiley-VCH Verlag GmbH & Co. KGaA, Weinheim, **2015**, pp. 315–339.

[5] C. Z. Wang, J. H. Lan, Q. Y. Wu, Y. L. Zhao, X. K. Wang, Z. F. Chai, W. Q. Shi, *Dalton Trans.* **2014**, *43*, 8713–8720.

[6] N. M. Atherton, *Principles of Electron Spin Resonance*, Ellis Horwood - Prentice Hall, New York, **1993**.

[7] F. Gendron, D. Páez-Hernández, F. P. Notter, B. Pritchard, H. Bolvin, J. Autschbach, *Chem. Eur. J.* **2014**, *20*, 7994–8011.

[8] F. P. Notter, H. Bolvin, *J. Chem. Phys.* **2009**, *130*, 184310–11.

[9] D. P. Hernández, H. Bolvin, *J. Electron Spectros. Relat. Phenomena* **2014**, *194*, 74–80.

[10] D. A. Case, *J. Chem. Phys.* **1985**, *83*, 5792–5796.

[11] R. Arratia-Pérez, L. Hernandez-Acevedo, G. L. Malli, *J. Chem. Phys.* **2004**, *121*, 7743–7747.

[12] R. Arratia-Pérez, G. L. Malli, *J. Chem. Phys.* **2006**, *124*, 74321–5.

[13] D. Ganyushin, F. Neese, *J. Chem. Phys.* **2013**, *138*, 104113–19.

[14] J. T. Coutinho, M. A. Antunes, L. C. J. Pereira, H. Bolvin, J. Marçalo, M. Mazzanti, M. Almeida, *Dalton Trans.* **2012**, *41*, 13568–13571.

[15] M. A. Antunes, I. C. Santos, H. Bolvin, L. C. J. Pereira, M. Mazzanti, J. Marçalo, M. Almeida, *Dalton Trans.* **2013**, *42*, 8861–8867.

[16] C. Boisson, J. C. Berthet, M. Lance, M. Nierlich, J. Vigner, M. Ephritikhine, *J. Chem. Soc. Chem. Commun.* **1995**, *25*, 543–544.

[17] C. Boisson, J. C. Berthet, M. Lance, J. Vigner, M. Nierlich, M. Ephritikhine, *J. Chem. Soc. Dalt. Trans.* **1996**, 947–953.

[18] T. Arliguie, M. Lance, M. Nierlich, J. Vigner, M. Ephritikhine, *J. Chem. Soc., Chem. Commun.* **1995**, *44*, 183–184.

[19] D. Gourier, D. Caurant, J. C. Berthet, C. Boisson, M. Ephritikhine, *Inorg. Chem.* **1997**, *36*, 5931–5936.

[20] D. Gourier, D. Caurant, T. Arliguie, M. Ephritikhine, *J. Am. Chem. Soc.* **1998**, *120*, 6084–6092.

[21] G. Schreckenbach, T. Ziegler, *J. Phys. Chem. A* **1997**, *101*, 3388–3399.

[22] E. van Lenthe, A. van der Avoird, P. E. S. Wormer, *J. Chem. Phys.* **1997**, *107*, 2488–2498.

[23] G. Schreckenbach, T. Ziegler, *Theor. Chem. Acc.* **1998**, *99*, 71–82.

[24] V. G. Malkin, M. Kaupp, *J. Am. Chem. Soc.* **2000**, *122*, 9206–9218.

[25] S. Patchkovskii, T. Ziegler, *J. Phys. Chem. A* **2001**, *105*, 5490–5497.

[26] F. Neese, *J. Chem. Phys.* **2001**, *115*, 11080–11096.

[27] H. Bolvin, J. Autschbach, in *Handb. Relativ. Quantum Chem.* (Ed.: W. Lui), Springer-Verlag, Berlin Heidelberg, **2017**, pp. 725–763.

[28] H. Bolvin, *ChemPhysChem* **2006**, *7*, 1575–1589.

[29] L. F. Chibotaru, L. Ungur, *J. Chem. Phys.* **2012**, *137*, 64112–22.

[30] M. Filatov, *Chem. Phys. Lett.* **2002**, *365*, 222–231.

[31] J. H. van Lenthe, S. Faas, J. G. Snijders, *Chem. Phys. Lett.* **2000**, *328*, 107–112.

[32] D. A. Pantazis, F. Neese, *J. Chem. Theory Comput.* **2011**, *7*, 677–684.

[33] F. Weigend, R. Ahlrichs, *Phys. Chem. Chem. Phys.* **2005**, *7*, 3297–3305.

[34] G. E. Gaussian 09, Revision B.01, M. J. Frisch, G. W. Trucks, H. B. Schlegel, S. Scuseria, M. A. Robb, J. R. Cheeseman, G. Scalmani, V. Barone, B. Mennucci, G. A. Petersson, H. Nakatsuji, M. Caricato, X. Li, H. P. Hratchian, A. F. Izmaylov, J. Bloino, G. Zheng, J. L. Sonnenberg, M. Hada, M. Ehara, K. Toyota, R. Fukuda, J. Hasegawa, M., **n.d.**

[35] F. Neese, *Wiley Interdiscip. Rev. Comput. Mol. Sci.* **2012**, *2*, 73–78.

[36] B. A. Hess, *Phys. Rev. A* **1985**, *32*, 756–763.

[37] G. Jansen, B. A. Hess, *Phys. Rev. A* **1989**, *39*, 6016–6017.

[38] P. Å. Malmqvist, B. O. Roos, B. Schimmelpfennig, *Chem. Phys. Lett.* **2002**, *357*, 230–240.

[39] F. Neese, *J. Chem. Phys.* **2005**, *122*, 34107–13.

[40] B. Sandhoefer, F. Neese, *J. Chem. Phys.* **2012**, *137*, 94102–15.

[41] J. Li, B. E. Bursten, **1997**, *2*, 9021–9032.

[42] S. H. Vosko, L. Wilk, M. Nusair, *Can. J. Phys.* **1980**, *58*, 1200–1211.

[43] A. D. Becke, *Phys. Rev. A* **1988**, *38*, 3098–3100.

[44] J. P. Perdew, *Phys. Rev. B* **1986**, *33*, 8822–8824.

[45] J. P. Perdew, K. Burke, M. Ernzerhof, *Phys. Rev. Lett.* **1996**, *77*, 3865–3868.

[46] J. P. Perdew, K. Burke, M. Ernzerhof, *Phys. Rev. Lett.* **1997**, *78*, 1396.

[47] V. N. Staroverov, G. E. Scuseria, J. Tao, J. P. Perdew, *J. Chem. Phys.* **2003**, *119*, 12129–12137.

[48] A. D. Becke, *J. Chem. Phys.* **1993**, *98*, 1372–1377.

[49] C. Lee, W. Yang, R. G. Parr, *Phys. Rev. B* **1988**, *37*, 785–789.

[50] P. J. Stephens, F. J. Devlin, C. F. Chabalowski, M. J. Frisch, *J. Phys. Chem.* **1994**, *98*, 11623–1627.

[51] C. Adamo, V. Barone, *J. Chem. Phys.* **1999**, *110*, 6158–6170.

[52] P. Pulay, T. P. Hamilton, *J. Chem. Phys.* **1988**, *88*, 4926–4933.

[53] F. Neese, E. I. Solomon, *Inorg. Chem.* **1998**, *37*, 6568–6582.

[54] S. Vancoillie, P. Malmqvist, K. Pierloot, *ChemPhysChem* **2007**, *8*, 1803–1815.

10.1002/chem.201701058

WILEY-VCH

Entry for the Table of Contents (Please choose one layout)

Layout 1:

FULL PAPER

Useful accuracy can be obtained for the **g** tensors of U(V) complexes using relatively simple and well-established quantum chemical methods. By carrying out small geometric perturbations of the molecular structures we are able to delineate the key features of the underlying structure that influence the computed values. This allows us to relate the changes in electronic structure with the changes in the *g* values, providing a simple physical picture of these subtle molecular properties.

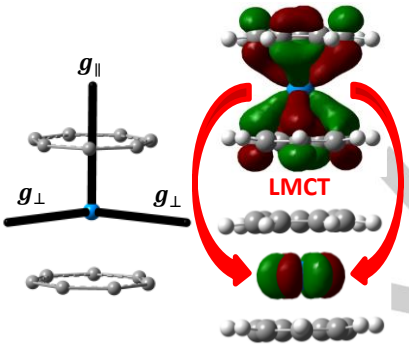

H.M Moylan, J.J.W McDouall*

Page No. – Page No.

Electronic g Tensors in U(V) Complexes - A Computational Study